Electronic Supporting Information (ESI)

Hybrid Trimetallic–Organic Framework-derived N, C co-doped Ni-Fe-Mn−P Ultrathin Nanosheet Electrocatalyst for Proficient Overall Water-splitting

Ram Babu Ghising [a], Uday Narayan Pan [a], Dasu Ram Paudel [a], Mani Ram Kandel [a], Nam Hoon Kim [a, *], and Joong Hee Lee [a, b, *]

[a] Department of Nano Convergence Engineering (BK21 Four), Jeonbuk National University, Jeonju, Jeonbuk, 54896, Republic of Korea.

[b] Carbon Composite Research Centre, Department of Polymer-Nano Science and Technology, Jeonbuk National University, Jeonju, Jeonbuk, 54896, Republic of Korea.

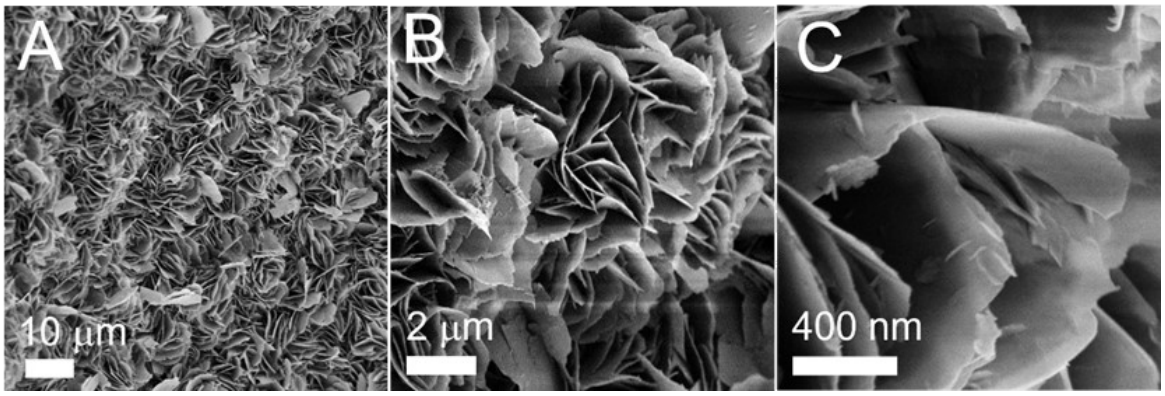

Fig. S1. (**A-C**) FE-SEM imagery of trimetallic-organic framework Ni-Fe-Mn-MOF@NF from low to high magnifications.

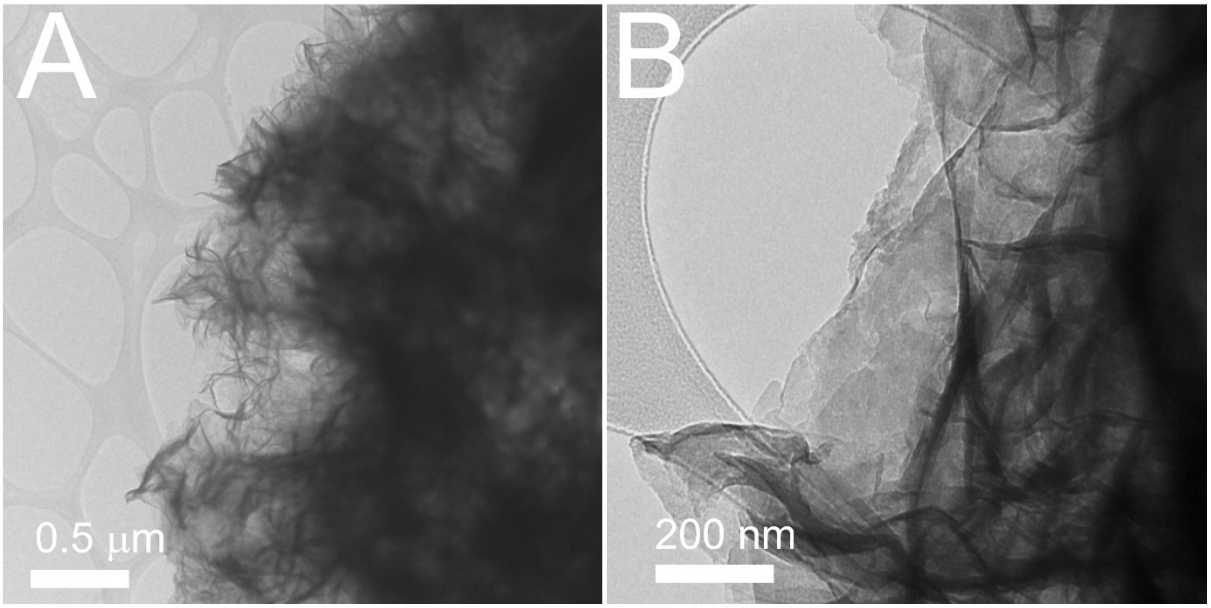

Fig. S2. (A&B) TEM imagery of trimetallic-organic framework Ni-Fe-Mn-MOF@NF from low to high magnifications.

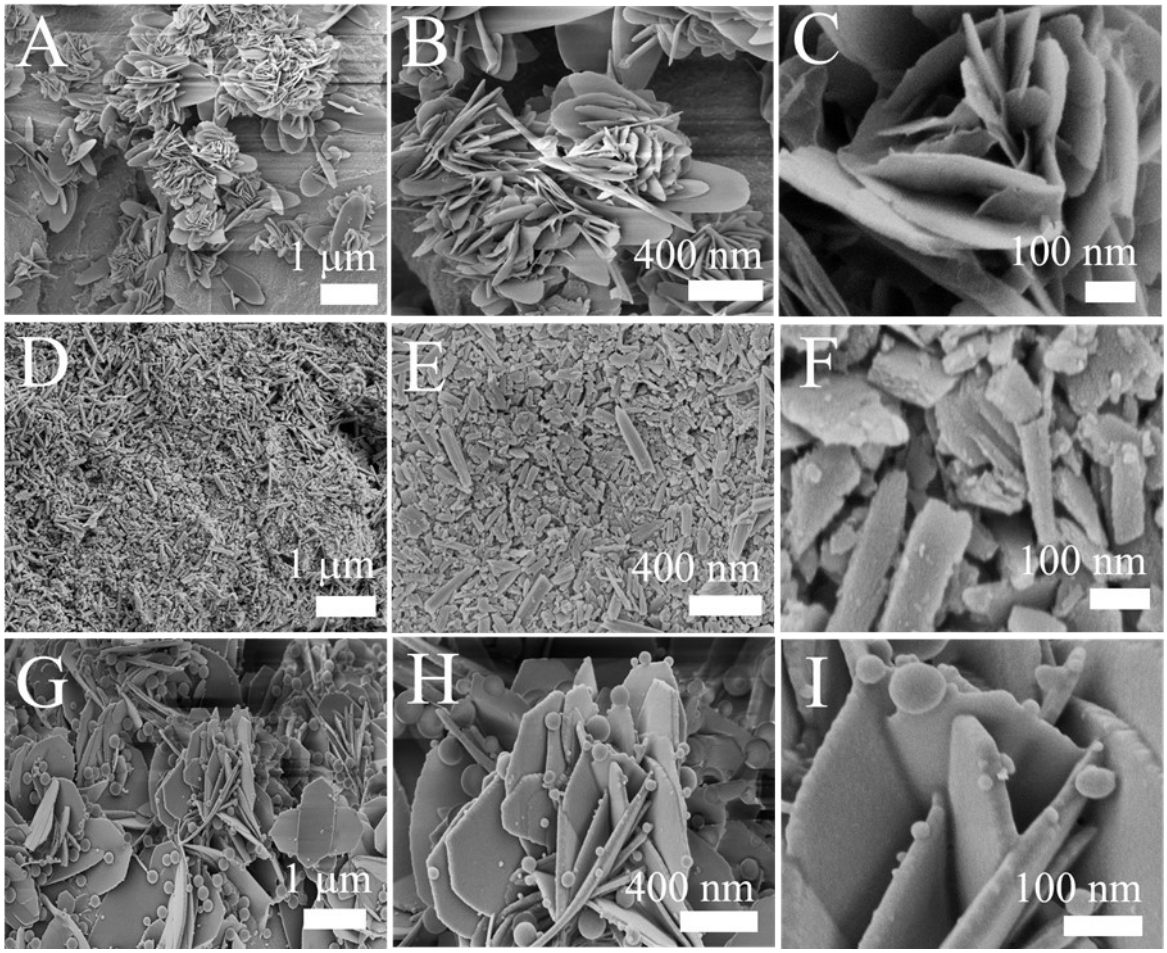

Fig. S3. FE-SEM imagery of (**A-C**) Ni-MOF@NF, (**D-F**) Fe-MOF@NF and (**G-I**) Mn-MOF@NF from low to high magnifications.

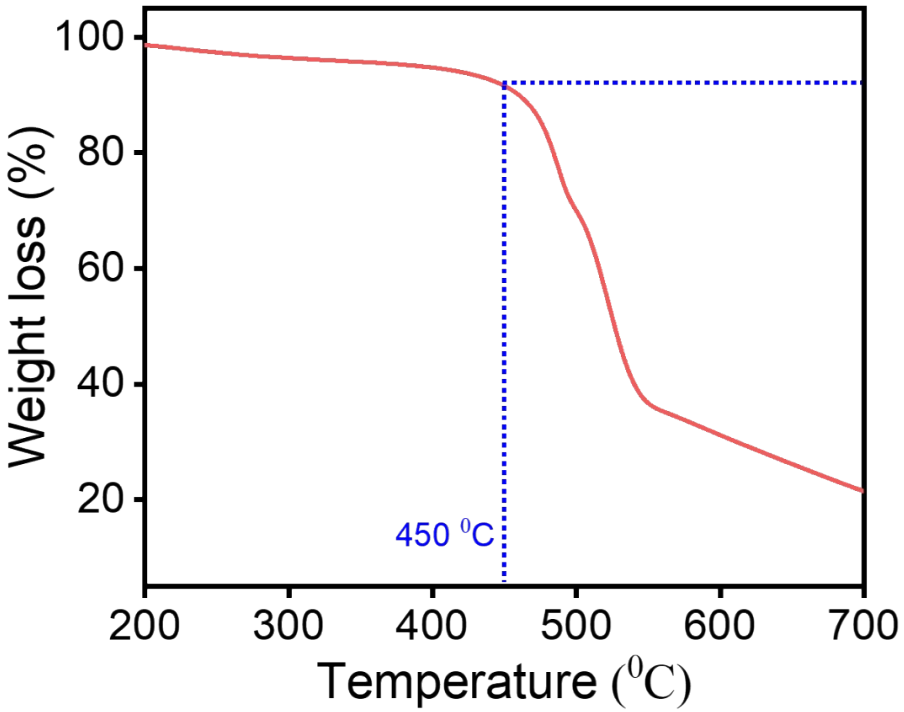

Fig. S4. Thermogravimetric analysis (TGA) of Ni-Fe-Mn-MOF

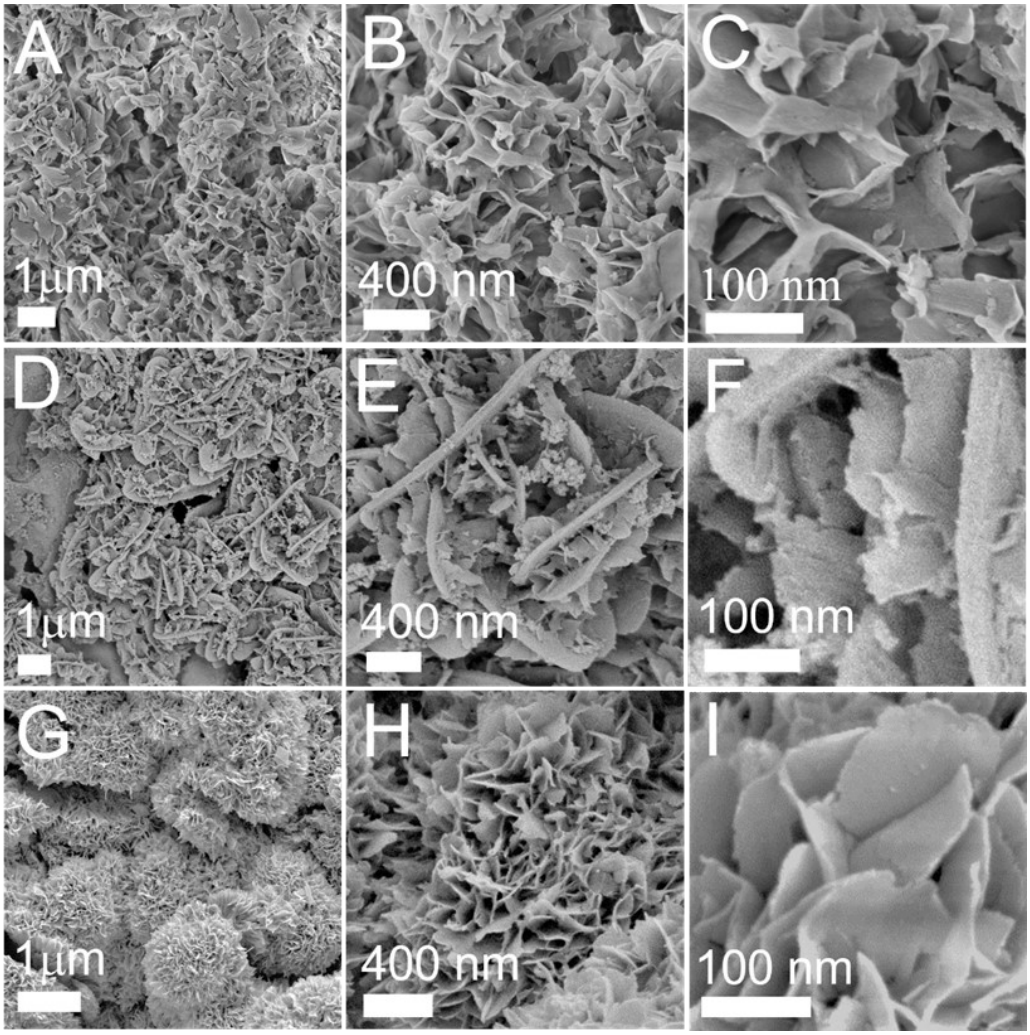

Fig. S5. FE-SEM imagery of (**A-C**) Ni_2P/NC@NF, (**D-F**) FeP/NC@NF and (**G-I**) MnP/NC@NF from low to high magnifications.

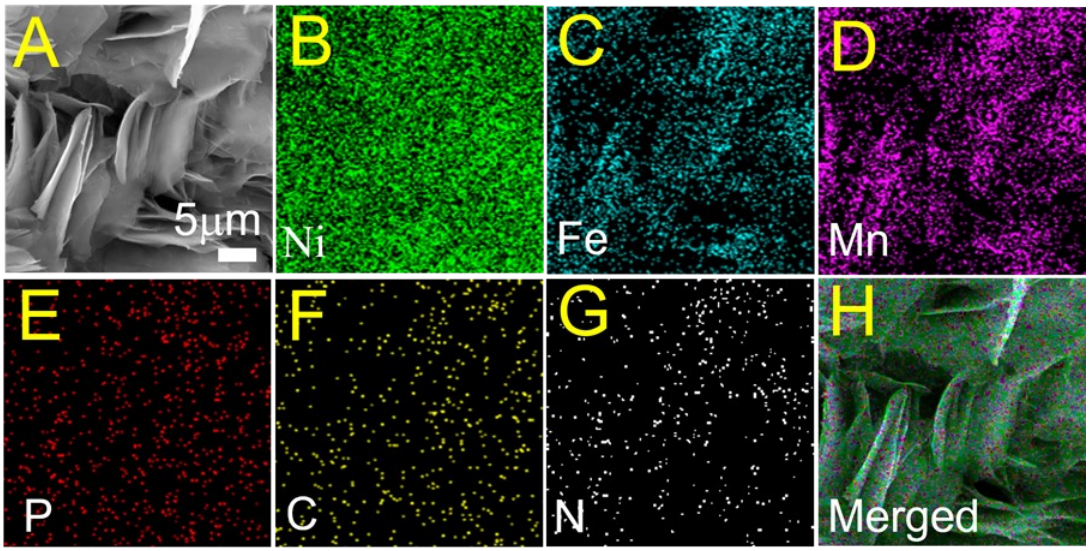

Fig. S6. (**A**) FE-SEM imagery, (**B-G**) SEM-EDX elemental color mappings corresponding to Ni, Fe, Mn, P, C and N of Ni-Fe-Mn-P/NC@NF respectively, and (**H**) merged color mappings of constituent elements of Ni-Fe-Mn-P/NC@NF.

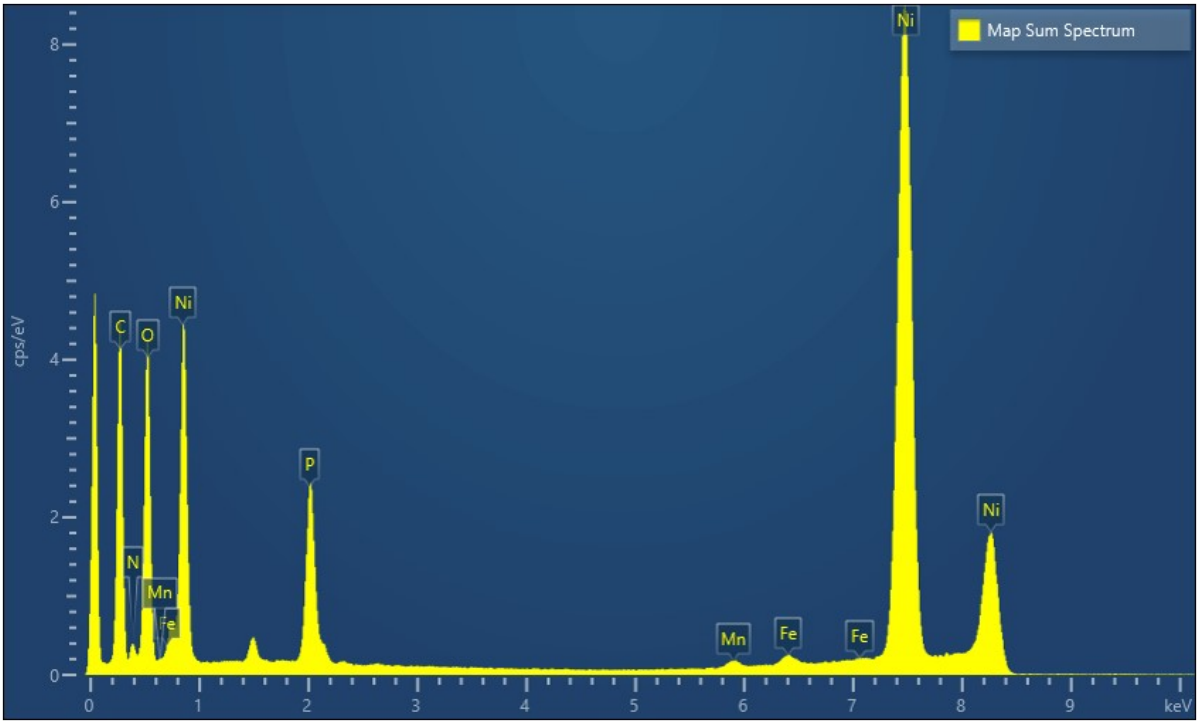

Fig. S7. SEM-EDX spectra of Ni-Fe-Mn-P/NC@NF.

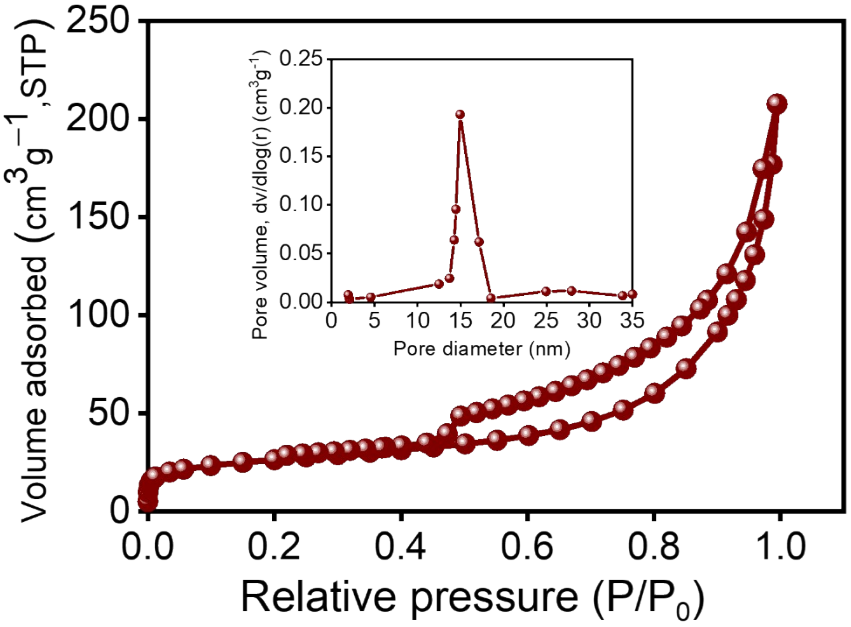

Fig. S8. Nitrogen adsorption-desorption isotherm and pore-size distribution (inset) of Ni-Fe-Mn-MOF@NF.

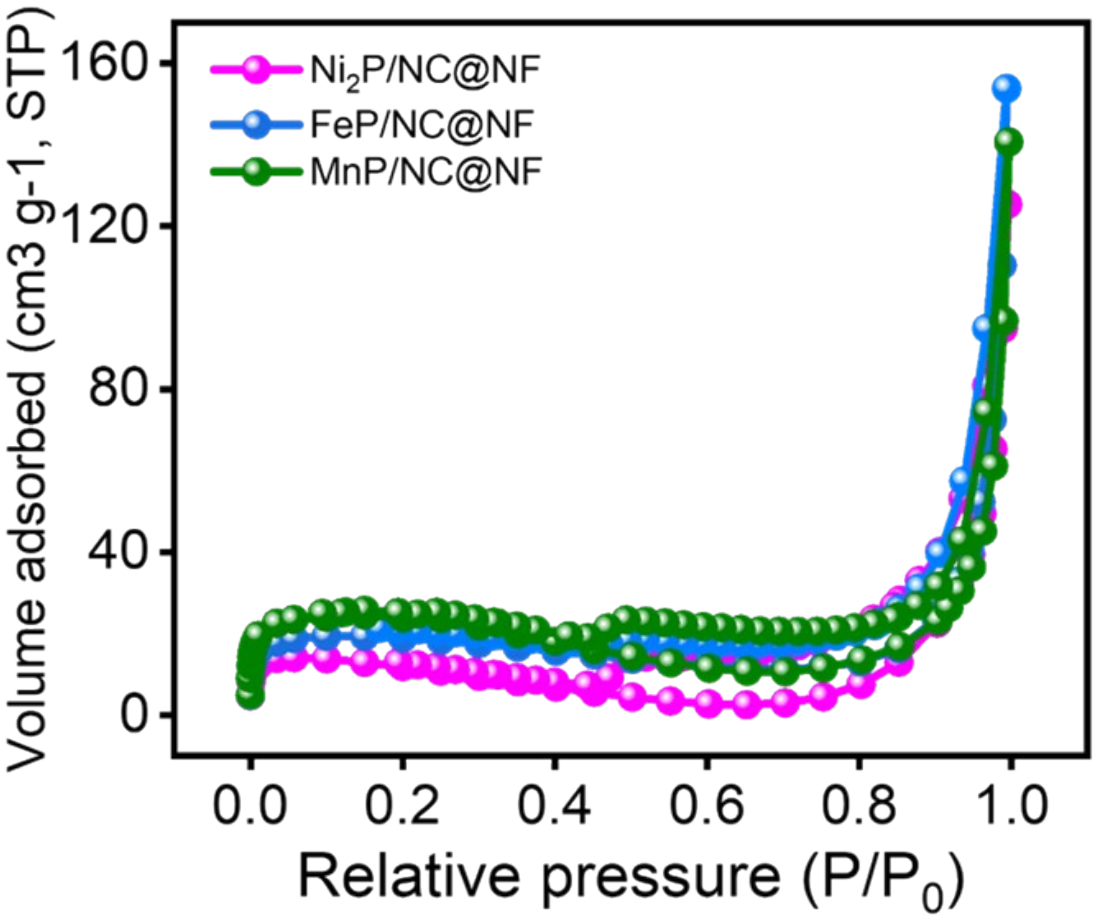

Fig. S9. Brunauer-Emmette-Teller (BET) specific surface area of Ni_2P/NC@NF, FeP/NC@NF and MnP/NC@NF.

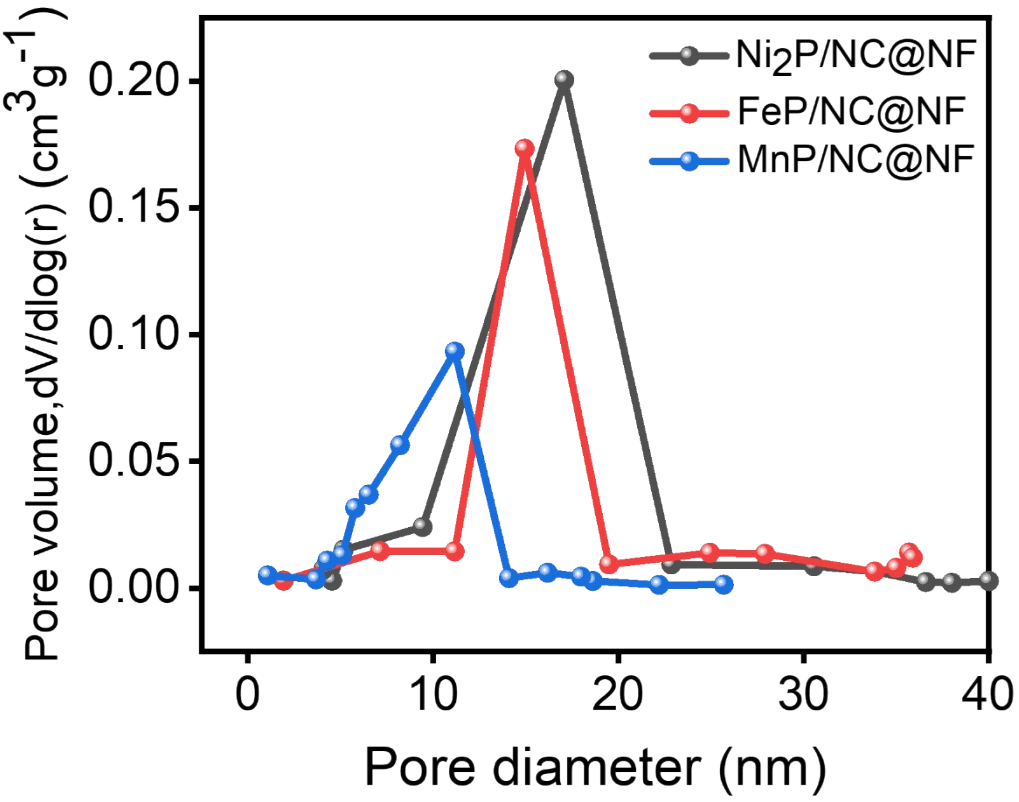

Fig. S10. Barrett-Joyner-Halenda (BJH) pore size distribution of Ni_2P/NC@NF, FeP/NC@NF and MnP/NC@NF.

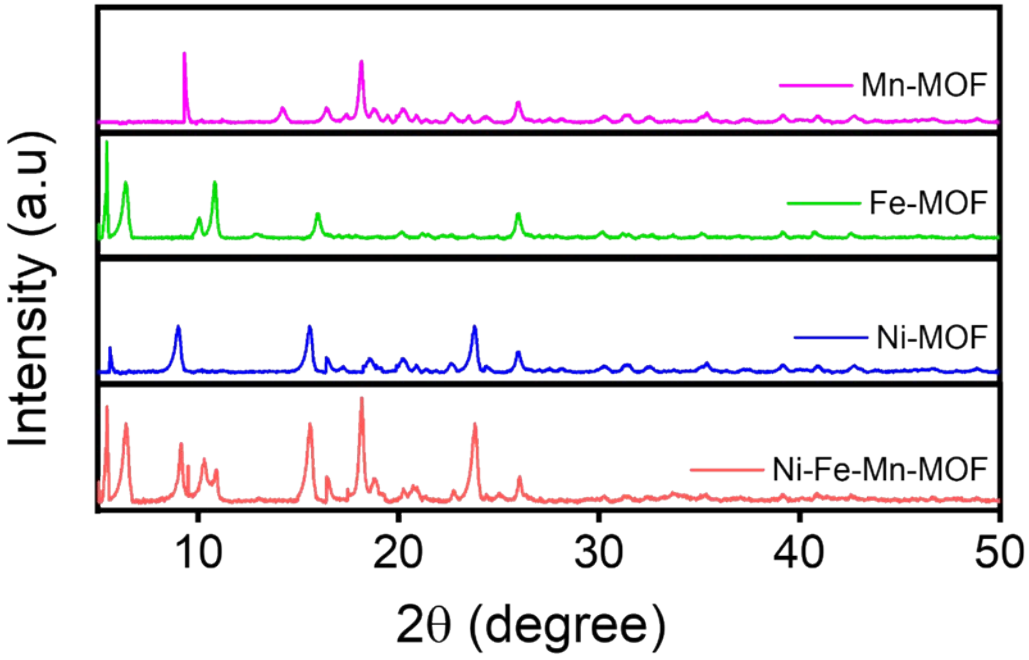

Fig. S11. Powder XRD (PXRD) patterns of Ni-Fe-Mn-MOF, Ni-MOF, Fe-MOF and Mn-MOF.

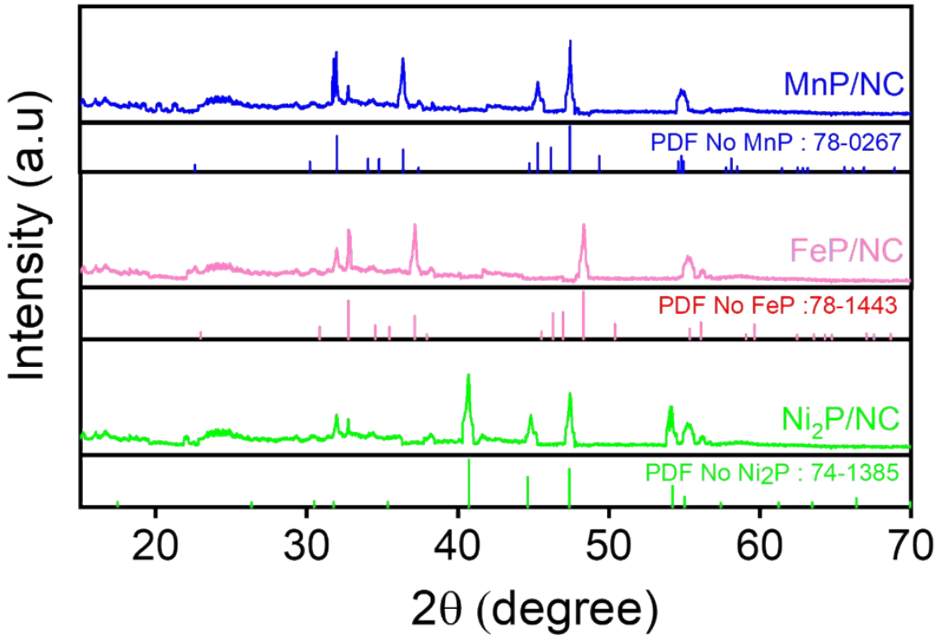

Fig. S12. Powder XRD (PXRD) patterns of Ni_2P/NC, FeP/NC and MnP/NC.

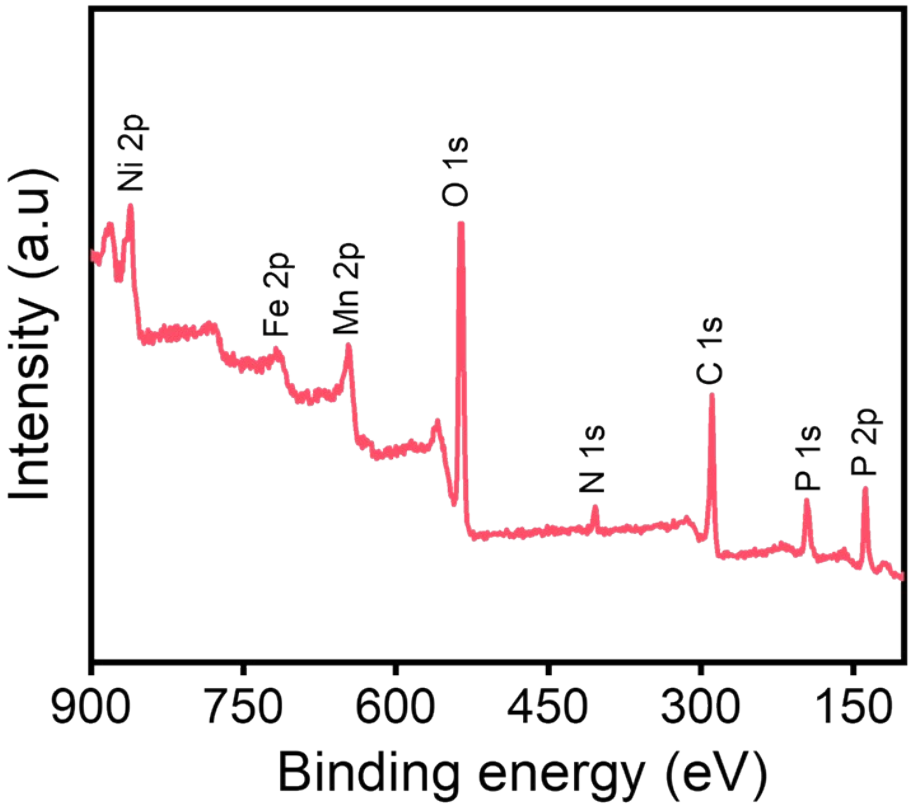

Fig. S13. X-ray photoelectron spectroscopy (XPS) survey spectrum of Ni-Fe-Mn-P/NC.

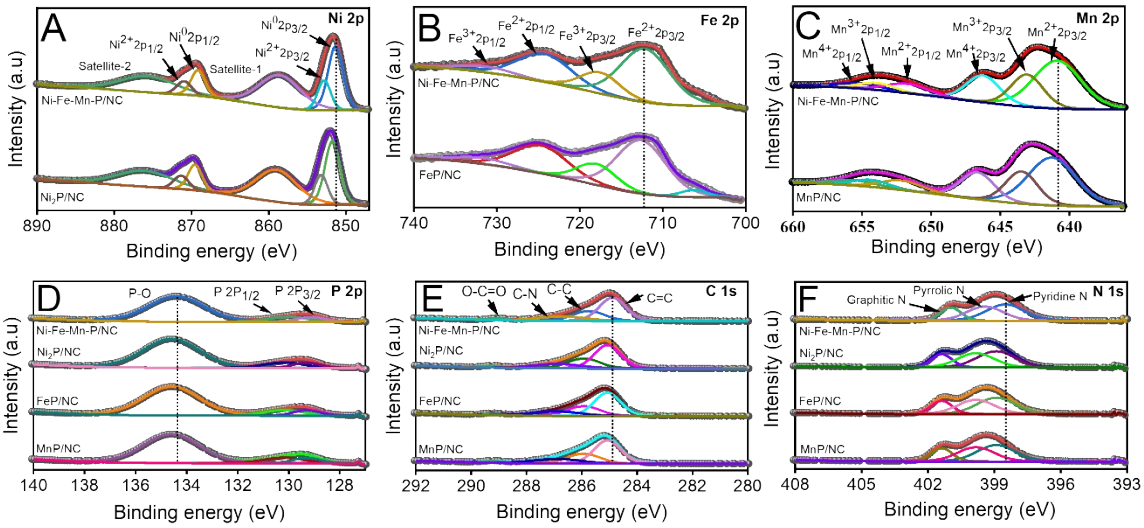

Fig. S14. Comparison of high-resolution X-ray photoelectron spectroscopy (HR-XPS) spectra of **(A)** Ni 2p **(B)** Fe 2p **(C)** Mn 2p **(D)** P 2p **(E)** C 1s and **(F)** N 1s of Ni-Fe-Mn-P/NC with Ni_2P/NC, FeP/NC and MnP/NC respectively.

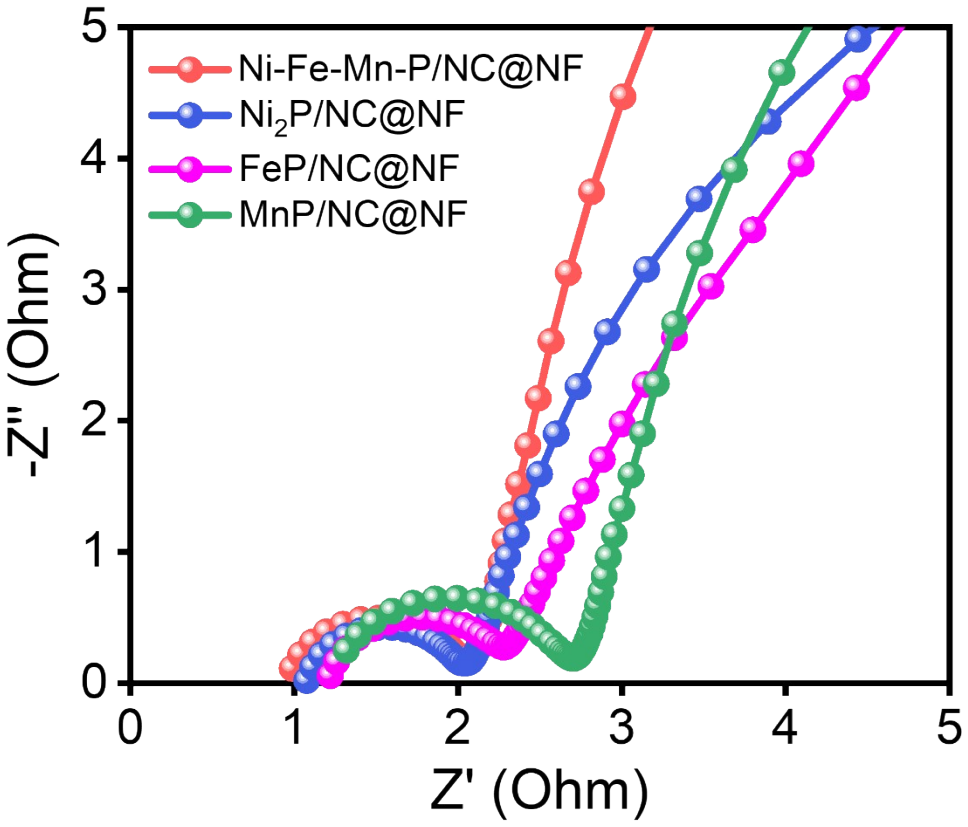

Fig. S15. Electrochemical impedance spectroscopy (EIS) measurements of Ni-Fe-Mn-P/NC@NF, Ni_2P/NC@NF, FeP/NC@NF and MnP/NC@NF to study charge transfer mechanism.

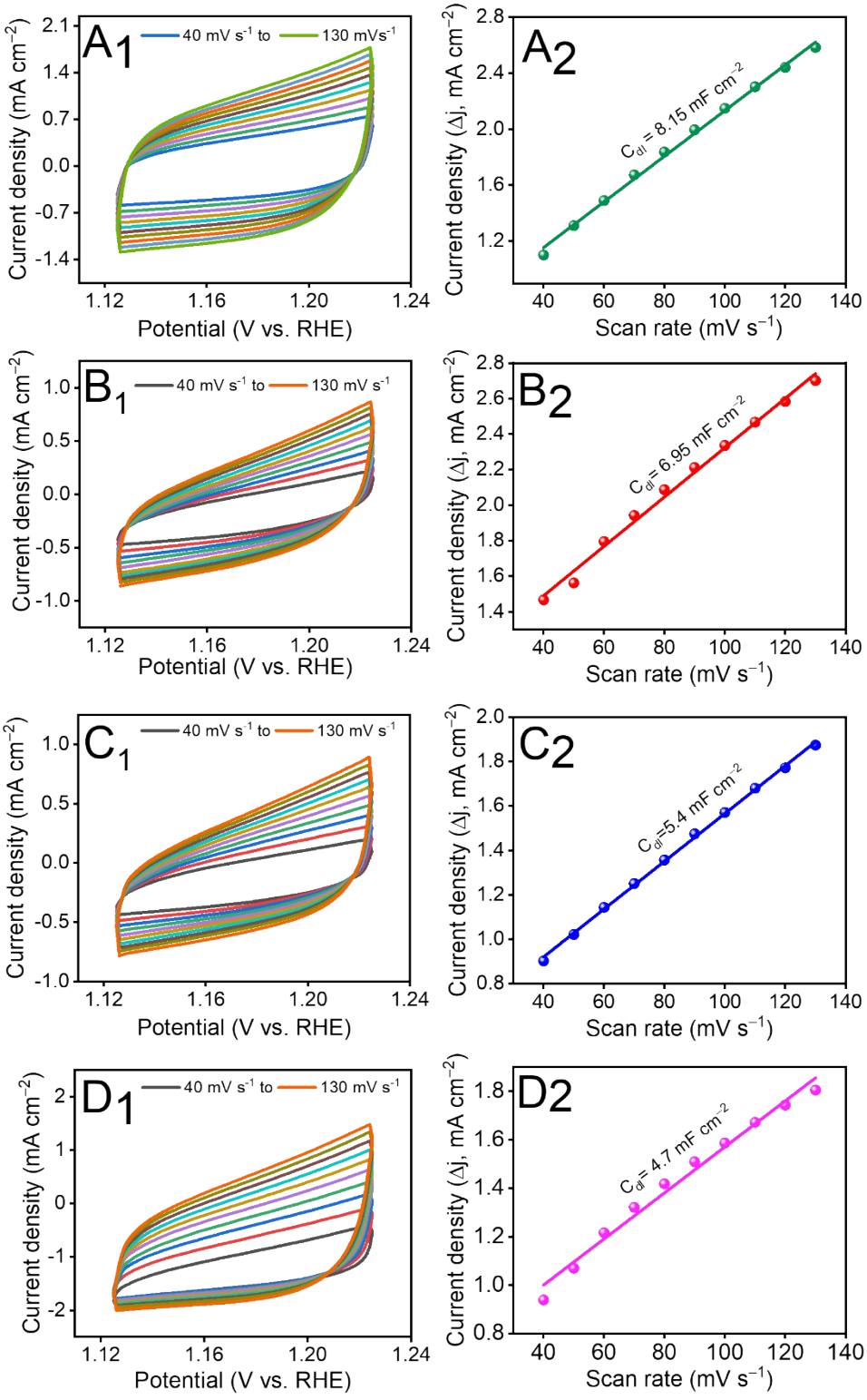

Fig. S16. Cyclic voltammetry (CV) curves at scan rates from 40 mV s^{-1} to 130 mV s^{-1} and their corresponding capacitance double layer values of (**A_1 & A_2**) Ni-Fe-Mn-P/NC@NF, (**B_1 & B_2**) Ni_2P/NC@NF, (**C_1 & C_2**) FeP/NC@NF and (**D_1 & D_2**) MnP/NC@NF respectively.

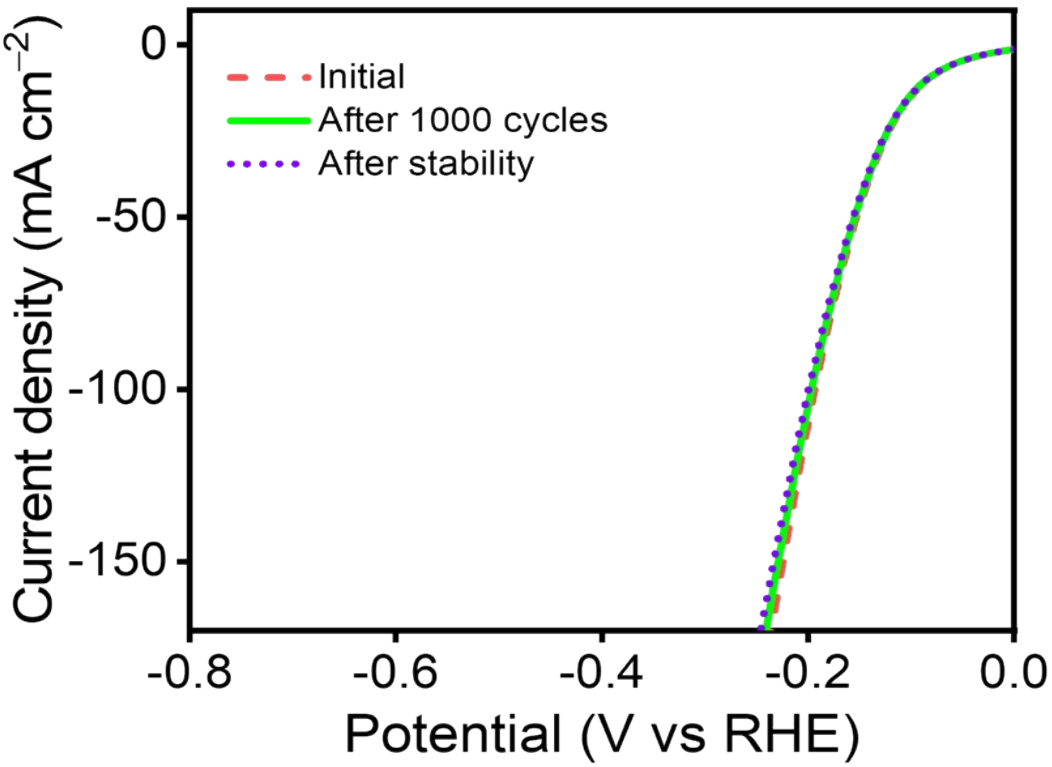

Fig. S17. Linear sweep voltammetry (LSV) curves towards HER demonstrating initial, after 1000 consecutive cyclic voltammetry cycles and after chronopotentiometry stability test of Ni-Fe-Mn-P/NC@NF.

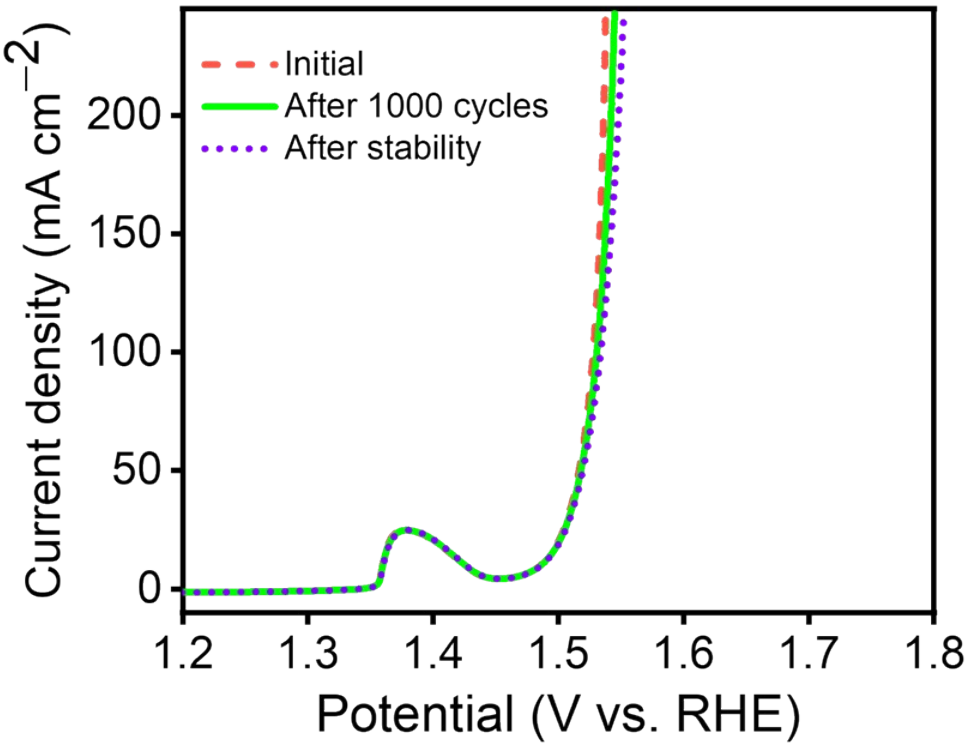

Fig. S18. Linear sweep voltammetry (LSV) curves for OER at initial, after 1000 consecutive cyclic voltammetry cycles and after chronopotentiometry stability test of Ni-Fe-Mn-P/NC@NF.

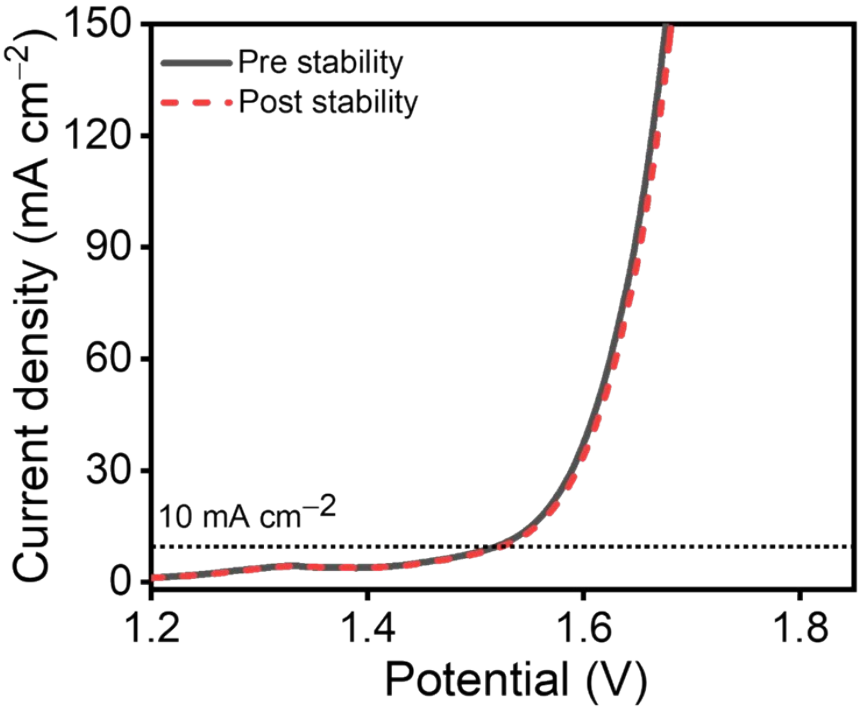

Fig. S19. Polarization curves of device Ni-Fe-Mn-P/NC@NF (+, -) demonstrating pre and post amperometric i-t stability test.

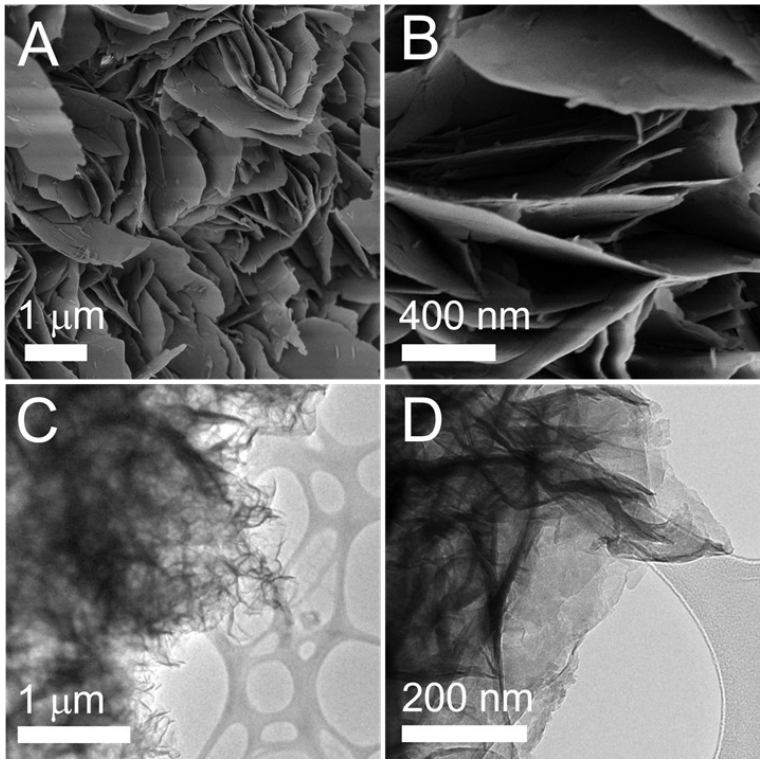

Fig. S20. (**A-B**) FE-SEM imagery and (**C-D**) TEM imagery of Ni-Fe-Mn-P/NC after amperometric i-t stability test, from low to high magnifications.

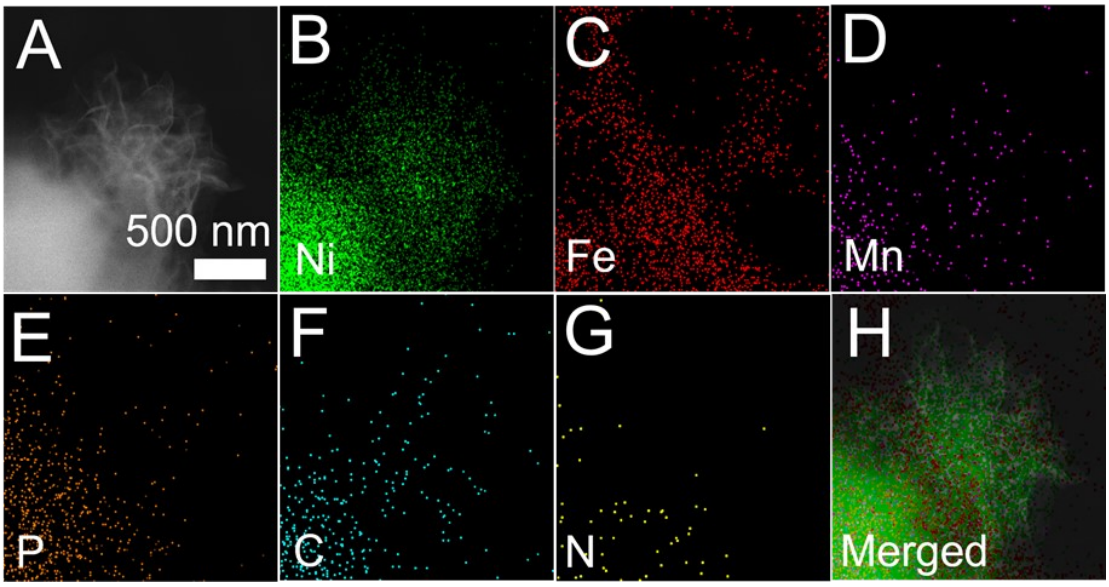

Fig. S21. (**A**) STEM imagery, (**B-G**) color mappings of constituent elements Ni, Fe, Mn, P, C and N of Ni-Fe-Mn-P/NC respectively and (**H**) merged color mappings of constituent elements of Ni-Fe-Mn-P/NC after amperometric i-t stability test.

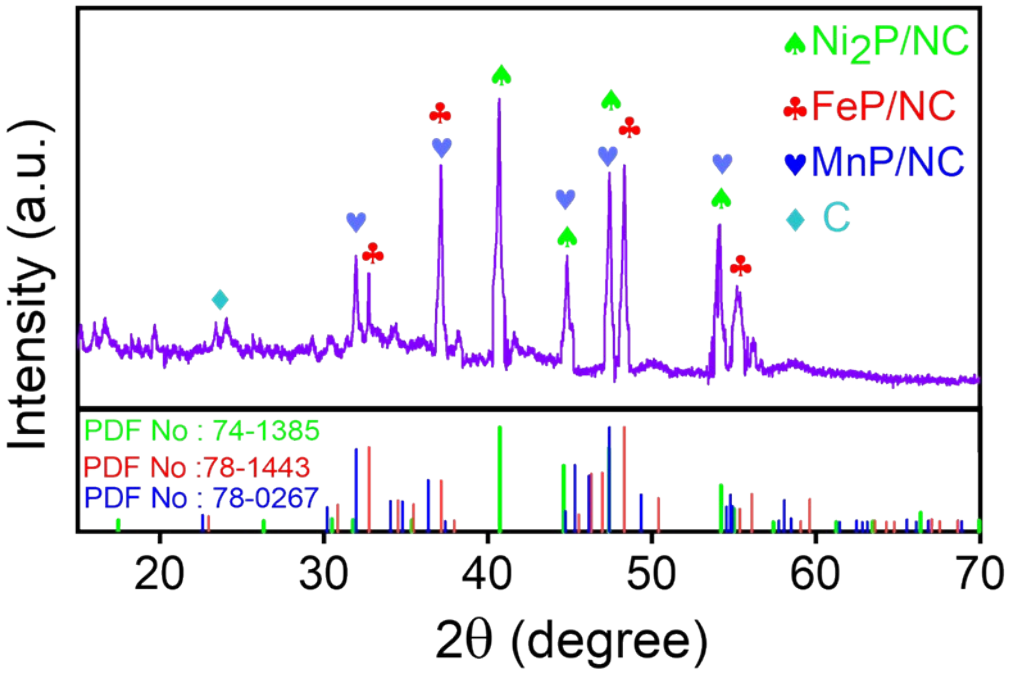

Fig. S22: Powder XRD (PXRD) patterns of Ni-Fe-Mn-P/NC@NF after amperometric i-t stability test.

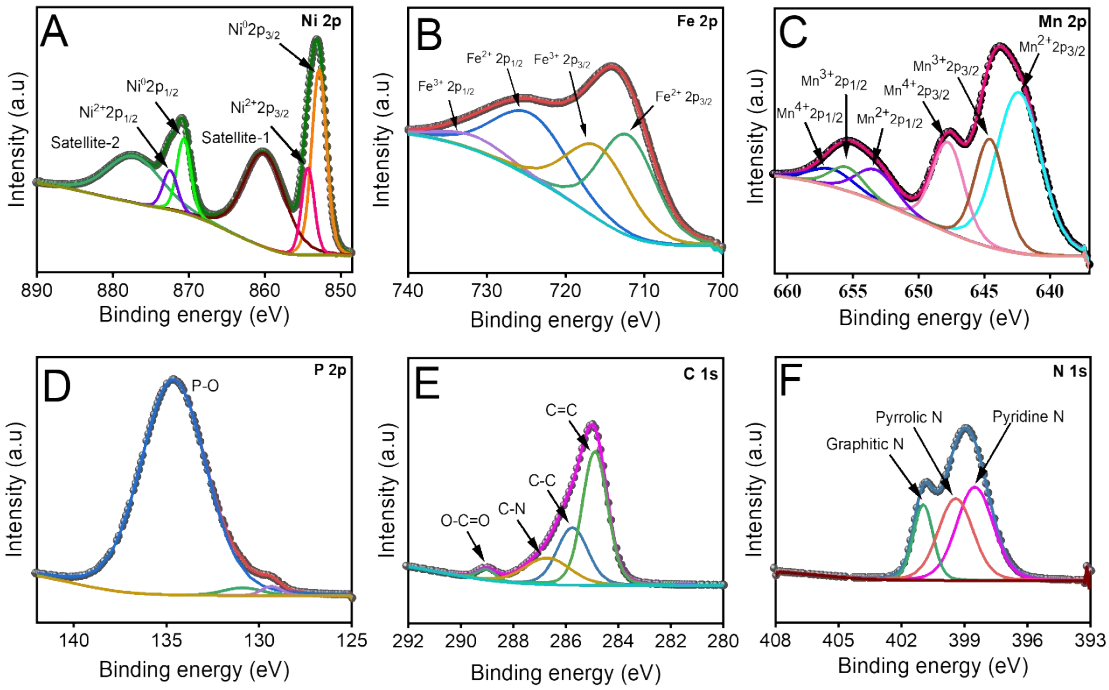

Fig. S23. High-resolution X-ray photoelectron spectroscopy (HR-XPS) spectra of **(A)** Ni 2p, **(B)** Fe 2p, **(C)** Mn 2p, **(D)** P 2p, and **(E)** C 1s and **(F)** N 1s of Ni-Fe-Mn-P/NC@NF after amperometric i-t stability test.

Table S1. Elemental composition of the Ni-Fe-Mn-P/NC resulted from inductively coupled plasma mass spectrometry (ICP-MS) analysis.

Sample Ni-Fe-Mn -P/NC	Ni Atomic %	Fe Atomic %	Mn Atomic %	P Atomic %	C Atomic %	N Atomic %
ICP-MS	29.6	14.1	13.9	23.4	16.4	2.6

Table S2. Tafel slope values and HER mechanism

Materials	**Tafel slope values**	**Reaction mechanism**
Pt-C@NF	29.4 mV dec^{-1}	Volmer-Tafel reaction
Ni-Fe-Mn-P@NF	79.8 mV dec^{-1}	Volmer-Heyrovsky reaction
Ni_2P@NF	98.8 mV dec^{-1}	Volmer-Heyrovsky reaction
FeP@NF	121.4 mV dec^{-1}	Volmer-Heyrovsky reaction
MnP@NF	152.7 mV dec^{-1}	Volmer-Heyrovsky reaction

Table S3: Comparison of HER activity of Ni-Fe-Mn-P/NC@NF with other recently reported

Electrocatalysts	Overpotential (mV) @ 10 mA cm^{-2}	References
Ni-Fe-Mn–P/NC@NF	72	This work
MOF-derived NiFeOx@C	189	[1]
MOF derived Ni-M@C-130	123	[2]
MOF-derived Co_3Fe_7@NCNTFs	197	[3]
MOF-derived Co-NCNTFs//NF	140	[4]
CoNiBDC/CC	135	[5]
MOF-derived CoS@CoNi-LDH/CC	124	[6]
$Ni_3(Ni_3{\cdot}HAHATN)_2$ MOF	115	[7]
NiFe(dobpdc)	113	[8]
FeCoMnNi-MOF-74/NF	108	[9]
$Mn_{0.52}Fe_{0.71}$Ni-MOF-74	99	[10]
MOF-derived CC-NC-NiFeP	94	[11]

MOF-based electrocatalysts.

Table S4: Comparison of OER activity of Ni-Fe-Mn-P/NC@NF with other recently reported

Electrocatalysts	Overpotential (mV) @10 mA cm^{-2}	References
Ni-Fe-Mn–P/NC@NF	274 @ 30 mA cm^{-2}	This work
MOF-derived Co-MOF/H_2	312	[12]
MOF derived HXP@NC800	307	[13]
MOF-derived MCF/NPCCNT-40	292	[14]
2D Ni-BDC/Ni $(OH)_2$	320	[15]
MOF-derived CoS_2	298	[16]
MOF-derived NCMC	290	[17]
Fe-MOF/NF	370	[18]
MOF-derived Fe_1Co_2-P/C	362	[19]
MOF-derived CoDNi-N/C	360	[20]
MOF-derived Cu@CuO-C	340	[21]
$A_{2.7}$B-MOF-$FeCo_{1.6}$	288	[22]

MOF-based electrocatalysts.

Table S5: Comparison of cell voltage of Ni-Fe-Mn-P/NC@NF (+, -) device with other recently reported MOF-based bifunctional electrocatalysts.

Bifunctional electrocatalysts	Cell voltage (V) @ 10 mA cm^{-2}	References
Ni-Fe-Mn–P/NC@NF (+, –)	1.52	This work
MOF-derived Ni-M@C-130 (+, –)	1.565	[2]
MOF-derived $NiFeO_x$@C (+, –)	1.59	[1]
MOF-derived Co–MOF/H_2 (+, –)	1.691	[12]
MOF-derived Co/NBC-900 (+, –)	1.68	[23]
MOF-derived Co_3Fe_7@NCNTFs (+, –)	1.64	[3]
MOF-derived Co-NCNTFs//NF (+, –)	1.62	[4]
MOF-derived NCMC (+, –)	1.63	[17]
Ni-ZIF/Ni-B@NF (+, –)	1.54	[24]
Co@N-CS/N-HCP@CC (+, –)	1.545	[25]
RuO_2/Co_3O_4–RuCo@NC (+, –)	1.66	[26]
MOF-derived CoS_2 (+, –)	1.65	[16]

References

1 X. Xu, T. Wang, M. Zheng, Y. Li, J. Shi, T. Tian, R. Jia and Y. Liu, *J. Alloys Compd.*, 2021, **875**, 159970.

2 K. Srinivas, Y. Chen, X. Wang, B. Wang, M. Karpuraranjith, W. Wang, Z. Su, W. Zhang and D. Yang, *ACS Sustain. Chem. Eng.*, 2021, **9**, 1920–1931.

3 Q. Yuan, Y. Yu, P. C. Sherrell, J. Chen and X. Bi, *Chem. - An Asian J.*, 2020, **15**, 1728–1735.

4 Q. Yuan, Y. Yu, Y. Gong and X. Bi, *ACS Appl. Mater. Interfaces*, 2020, **12**, 3592–3602.

5 X. J. Bai, H. Chen, Y. N. Li, L. Shao, J. C. Ma, L. L. Li, J. Y. Chen, T. Q. Wang, X. M. Zhang, L. Y. Zhang, Y. Fu and W. Qi, *New J. Chem.*, 2020, **44**, 1694–1698.

6 K. Ao, Q. Wei and W. A. Daoud, *ACS Appl. Mater. Interfaces*, 2020, **12**, 33595–33602.

7 H. Huang, Y. Zhao, Y. Bai, F. Li, Y. Zhang and Y. Chen, *Adv. Sci.*, , DOI:10.1002/advs.202000012.

8 L. Qi, Y. Q. Su, Z. Xu, G. Zhang, K. Liu, M. Liu, E. J. M. Hensen and R. Y. Y. Lin, *J. Mater. Chem. A*, 2020, **8**, 22974–22982.

9 M. Zhang, W. Xu, T. Li, H. Zhu and Y. Zheng, *Inorg. Chem.*, 2020, **59**, 15467–15477.

10 W. Zhou, Z. Xue, Q. Liu, Y. Li, J. Hu and G. Li, *ChemSusChem*, 2020, **13**, 5647–5653.

11 J. Bian, Z. Song, X. Li, Y. Zhang and C. Cheng, *Nanoscale*, 2020, **12**, 8443–8452.

12 Q. Xia, H. Liu, M. Jin, L. Lai, Y. Qiu, H. Zhai, H. Li and X. Liu, *Nanoscale*, 2020, **12**, 8969–8974.

13 Y. Lin, H. Wan, D. Wu, G. Chen, N. Zhang, X. Liu, J. Li, Y. Cao, G. Qiu and R. Ma, *J.*

Am. Chem. Soc., 2020, **142**, 7317–7321.

14 X. Zhang, Y. Chen, M. Chen, B. Yu, B. Wang, X. Wang, W. Zhang and D. Yang, *J. Colloid Interface Sci.*, 2021, **581**, 608–618.

15 D. Zhu, J. Liu, L. Wang, Y. Du, Y. Zheng, K. Davey and S. Z. Qiao, *Nanoscale*, 2019, **11**, 3599–3605.

16 I. K. Ahn, W. Joo, J. H. Lee, H. G. Kim, S. Y. Lee, Y. Jung, J. Y. Kim, G. B. Lee, M. Kim and Y. C. Joo, *Sci. Rep.*, 2019, **9**, 1–10.

17 X. Wei, Y. Zhang, H. He, D. Gao, J. Hu, H. Peng, L. Peng, S. Xiao and P. Xiao, *Chem. Commun.*, 2019, **55**, 6515–6518.

18 X. Zhang, Q. Liu, X. Shi, A. M. Asiri and X. Sun, *Inorg. Chem. Front.*, 2018, **5**, 1405–1408.

19 W. Hong, M. Kitta and Q. Xu, *Small Methods*, 2018, **2**, 1–6.

20 Z. Li, H. He, H. Cao, S. Sun, W. Diao, D. Gao, P. Lu, S. Zhang, Z. Guo, M. Li, R. Liu, D. Ren, C. Liu, Y. Zhang, Z. Yang, J. Jiang and G. Zhang, *Appl. Catal. B Environ.*, 2019, **240**, 112–121.

21 J. X. Wu, C. T. He, G. R. Li and J. P. Zhang, *J. Mater. Chem. A*, 2018, **6**, 19176–19181.

22 Z. Xue, Y. Li, Y. Zhang, W. Geng, B. Jia, J. Tang, S. Bao, H. P. Wang, Y. Fan, Z. wen Wei, Z. Zhang, Z. Ke, G. Li and C. Y. Su, *Adv. Energy Mater.*, 2018, **8**, 1–7.

23 M. R. Liu, Q. L. Hong, Q. H. Li, Y. Du, H. X. Zhang, S. Chen, T. Zhou and J. Zhang, *Adv. Funct. Mater.*, 2018, **28**, 1–9.

24 H. Xu, B. Fei, G. Cai, Y. Ha, J. Liu, H. Jia, J. Zhang, M. Liu and R. Wu, *Adv. Energy Mater.*, 2020, **10**, 1–8.

25 Z. Chen, Y. Ha, H. Jia, X. Yan, M. Chen, M. Liu and R. Wu, *Adv. Energy Mater.*, 2019, **9**, 1–13.

26 Z. Fan, J. Jiang, L. Ai, Z. Shao and S. Liu, *ACS Appl. Mater. Interfaces*, 2019, **11**, 47894–47903.